DOI: 10.1002/ejic.200900760

Diphenoxido-Bridged Co^{II} and Zn^{II} Complexes of Tripodal N_2O_2 Ligands: Stabilisation of M^{II}-Coordinated Phenoxyl Radical Species

Atasi Mukherjee,[a] Francesc Lloret,[b] and Rabindranath Mukherjee*[a]

Keywords: Dinuclear complexes / Cobalt / Zinc / Phenol / Tripodal ligands / Solid-state structures / Redox chemistry / Density functional calculations

Three new tripodal ligands with an N_2O_2 donor set, namely 2-*tert*-butyl-6-({(2-hydroxybenzyl)[2-(2-pyridyl)ethyl]amino}-methyl)-4-methylphenol (H_2L^1), 2-*tert*-butyl-6-({(2-hydroxybenzyl)[2-(2-pyridyl)ethyl]amino}methyl)-4-methoxyphenol (H_2L^2) and 2-*tert*-butyl-6-({[2-(dimethylamino)ethyl]-(2-hydroxybenzyl)amino}methyl)-4-methoxyphenol (H_2L^3) have been synthesised. Treatment of the ligands with $Co(CH_3CO_2)_2{\cdot}4H_2O$ or $[Zn(H_2O)_6][ClO_4]_2$ in the presence of Et_3N provides the corresponding Co^{II} and Zn^{II} complexes of composition $[M^{II}_2(L^1)_2]$ [M = Co (**1**) (single-crystals are a solvate with the composition $[Co^{II}_2(L^1)_2]{\cdot}2CHCl_3$, i.e. **1**·2$CHCl_3$); M = Zn (**2**)], $[M^{II}_2(L^2)_2]$ [M = Co (**3**); Zn (**4**)] and $[Co^{II}_2(L^3)_2]$ (**5**). Crystallographic analyses reveal that the complexes have closely similar diphenoxido-bridged structures. Each metal centre assumes $M^{II}N_2O_3$ coordination. The geometry around each metal ion in **1**·2$CHCl_3$ (τ = 0.76), **2** (τ = 0.77), **3** (τ = 0.74), **4** (τ = 0.76) and **5** [one Co^{II} (τ = 0.49) and the other Co^{II} (τ = 0.63)] is intermediate between ideal square-pyramidal (τ = 0) and trigonal-bipyramidal (τ = 1). Temperature-dependent magnetic studies reveal weak intramolecular antiferromagnetic exchange couplings for all the three Co^{II} complexes ($-J$ = 1.84, 1.32 and 5.70 cm^{-1} for **1**, **3** and **5**, respectively). Spectroscopic properties of the complexes have also been investigated. Cyclic voltammetric (CV) measurements of **1** and **2** show an irreversible oxidative response at E_{pa} (anodic peak potential) in the range 0.60–0.75 V relative to the SCE (saturated calomel electrode), whereas two successive quasi-reversible oxidative responses can be observed for **3**–**5** at $E_{1/2}$ values in the range 0.40–0.53 V relative to the SCE. Oxidative responses are due to the formation of M^{II}-coordinated phenoxyl radical species. The metal-coordinated phenoxyl radical species, generated by two-electron coulometric oxidation of **3**–**5**, were characterised by CV and by adsorption and EPR spectroscopy. The stability of such species was determined by measuring the decay constant (absorption spectroscopy), which reveals that the phenoxyl radical species of **5** is more stable than that of **3** and **4**. EPR spectroscopic studies (120 K) of coulometrically generated two-electron oxidised species of **4** in CH_2Cl_2 (containing 0.1 M TBAP) at 298 K reveal a combination of an isotropic S = ½ signal at g = 2 [(phenolato)(phenoxyl radical)-coordinated dizinc(II) complex] and a spin-triplet resonance (S = 1) that gives rise to the symmetric split-line pattern [bis(phenoxyl radical)-coordinated dizinc(II) complex]. To pinpoint the site of oxidation (metal- or ligand-centred) in each case, DFT calculations were performed at the B3LYP level of theory.

Introduction

There has been growing interest in the development of coordination chemistry of metal-coordinated phenoxyl radical species due to their formation in the active sites of many metalloproteins.[1] Galactose oxidase is a mononuclear copper enzyme, which is an appropriate representation of good cooperativity[1b,1e,1j,2] between a metal ion and a radical for performing oxidation reactions.[3] A number of studies have been carried out to obtain information about the metal–radical interaction and also the stability/reactivity of metal-coordinated phenoxyl radical species.[4–10] As part of our general interest in extracting information on the stability/reactivity of metal-coordinated phenoxyl radical species, we recently reported the synthesis and characterisation of diphenoxido-bridged Co^{II}, Ni^{II}, Cu^{II} and Zn^{II} complexes with a common tripodal ligand providing an N_2O_2 donor set.[11] In continuation of this study, we address two aspects in this contribution, i.e. (i) the electronic effect of the substituent at the *p*-position of the terminal phenolato ring and (ii) the effect of chelate ring size on the stability of the phenoxyl radical species of the diphenoxido-bridged Co^{II} and Zn^{II} complexes with three new systematically varied tripodal ligands H_2L^1, H_2L^2 and H_2L^3 (Scheme 1). H_2L^1 possesses two phenol units (one unsubstituted and the other with a 2-*tert*-butyl and a 4-methyl substituent), an ethylpyridine unit and an aliphatic amine moiety. H_2L^2 differs from H_2L^1 (forms a six-membered chelate-ring) in its *p*-position on the substituted phenol unit, which is methoxy instead of methyl in H_2L^1. The pyridylethyl unit of H_2L^2

[a] Department of Chemistry, Indian Institute of Technology Kanpur,
Kanpur 208016, India
Fax: +91-512-2597437
E-mail: rnm@iitk.ac.in
[b] Departament de Química Inorgànica, Instituto de Ciencia Molecular (ICMOL), Universitat de València,
Polígono de la Coma, s/n, 46980 Paterna, València, Spain
Supporting information for this article is available on the WWW under http://dx.doi.org/10.1002/ejic.200900760.

(forms a six-membered chelate-ring) is replaced by a (dimethylamino)ethyl unit in H_2L^3 (forms a five-membered chelate-ring). This report presents an account of the synthesis, crystal structures, spectroscopic and magnetic properties, redox chemistry and studies on the generation and investigation of the stability of M^{II}-coordinated phenoxyl radical species (M^{II} = Co^{II} and Zn^{II}). To highlight the site of oxidation (metal- or ligand-centred) in each case, DFT calculations were performed at the B3LYP level of theory.

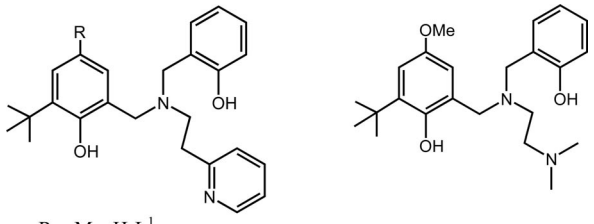

R = Me; H_2L^1
= OMe; H_2L^2

H_2L^3

Scheme 1. Ligands considered in this study.

Results and Discussion

Syntheses and General Characterisation

All three tripodal ligands H_2L^1–H_2L^3 (Scheme 1) were synthesised in a one-pot Mannich reaction (phenol and paraformaldehyde) followed by condensation with the corresponding amine in C_2H_5OH heated to reflux for 16 h. In the case of H_2L^1, the condensation reaction takes place between 2-({[2-(2-pyridinyl)ethyl]amino}methyl)phenol and 2-*tert*-butyl-4-methylphenol, whereas for the synthesis of H_2L^2, the latter phenol was replaced by 2-*tert*-butyl-4-methoxyphenol. However, for the synthesis of H_2L^3, 2-({[2-(dimethylamino)ethyl]amino}methyl)phenol and 2-*tert*-butyl-4-methoxyphenol were used. The new ligands were characterised by their ^1H NMR spectra. Notably, two kinds of phenol units (one unsubstituted and the other substituted) are present in these three ligands, and the [2-(2-pyridyl)-ethyl]amino moiety of H_2L^1 and H_2L^2 is replaced by the [2-(dimethylamino)ethyl]amino moiety in H_2L^3. Treatment of the ligands with appropriate Co^{II} and Zn^{II} salts in the presence of Et_3N enabled isolation of the complexes. Complexes **1**, **3** and **5** were isolated as pink powders under refluxing conditions, whereas complexes **2** and **4** were isolated as white solids at room temperature. ^1H NMR spectra of the diamagnetic complexes **2** and **4** are displayed in Figures S1 and S2, respectively (see Supporting Information).

Crystal Structures

In order to confirm the structures of the complexes and the modes of coordination of the deprotonated ligands, single-crystal X-ray structure determinations of the complexes were carried out. Selected bond lengths and bond angles are listed in Table 1.

Table 1. Selected bond lengths [Å] and angles [°] in **1**·2$CHCl_3$, **2**, **3**, **4** and **5**.

1·2$CHCl_3$			
Co(1)–O(1)	1.980(3)	Co(1)–O(1)–Co(1)[a]	100.23(11)
Co(1)–O(2)	1.918(3)	O(1)–Co(1)–O(2)	123.79(13)
Co(1)–O(1)[a]	2.109(3)	O(1)–Co(1)–O(1)[a]	79.77(11)
Co(1)–N(1)	2.185(3)	O(1)–Co(1)–N(1)	92.32(12)
Co(1)–N(2)	2.071(3)	O(1)–Co(1)–N(2)	109.91(13)
Co(1)···Co(2)	3.139(7)	O(2)–Co(1)–O(1)[a]	94.58(11)
		O(2)–Co(1)–N(1)	90.86(12)
		O(2)–Co(1)–N(2)	126.30(13)
		O(1)[a]–Co(1)–N(1)	171.99(12)
		O(1)[a]–Co(1)–N(2)	94.66(12)
		N(1)–Co(1)–N(2)	86.82(13)
2			
Zn(1)–O(1)	2.009(3)	Zn(1)–O(1)–Zn(1)[a]	101.64(13)
Zn(1)–O(2)	1.965(3)	O(1)–Zn(1)–O(2)	123.16(13)
Zn(1)–O(1)[a]	2.151(3)	O(1)–Zn(1)–O(1)[a]	78.36(13)
Zn(1)–N(1)	2.214(4)	O(1)–Zn(1)–N(1)	93.64(13)
Zn(1)–N(2)	2.106(4)	O(1)–Zn(1)–N(2)	111.97(14)
Zn(1)···Zn(2)	3.226(9)	O(2)–Zn(1)–O(1)[a]	97.68(12)
		O(2)–Zn(1)–N(1)	90.76(13)
		O(2)–Zn(1)–N(2)	124.71(14)
		O(1)[a]–Zn(1)–N(1)	170.64(12)
		O(1)[a]–Zn(1)–N(2)	88.94(13)
		N(1)–Zn(1)–N(2)	89.58(15)
3			
Co(1)–O(1)	1.987(3)	Co(1)–O(1)–Co(1)[a]	101.22(12)
Co(1)–O(2)	1.937(3)	O(1)–Co(1)–O(2)	120.77(14)
Co(1)–O(1)[a]	2.143(3)	O(1)–Co(1)–O(1)[a]	78.78(12)
Co(1)–N(1)	2.207(4)	O(1)–Co(1)–N(1)	92.58(13)
Co(1)–N(2)	2.110(4)	O(1)–Co(1)–N(2)	91.33(13)
Co(1)···Co(2)	3.193(9)	O(2)–Co(1)–O(1)[a]	97.32(13)
		O(2)–Co(1)–N(1)	90.08(14)
		O(2)–Co(1)–N(2)	126.17(14)
		O(1)[a]–Co(1)–N(1)	170.68(13)
		O(1)[a]–Co(1)–N(2)	91.33(13)
		N(1)–Co(1)–N(2)	88.85(15)
4			
Zn(1)–O(1)	1.996(4)	Zn(1)–O(1)–Zn(1)[a]	101.8(2)
Zn(1)–O(2)	1.963(5)	O(1)–Zn(1)–O(2)	122.55(19)
Zn(1)–O(1)[a]	2.130(5)	O(1)–Zn(1)–O(1)[a]	78.2(2)
Zn(1)–N(1)	2.207(6)	O(1)–Zn(1)–N(1)	92.7(2)
Zn(1)–N(2)	2.124(5)	O(1)–Zn(1)–N(2)	113.1(2)
Zn(1)···Zn(2)	3.203(9)	O(2)–Zn(1)–O(1)[a]	98.0(2)
		O(2)–Zn(1)–N(1)	91.0(2)
		O(2)–Zn(1)–N(2)	124.3(2)
		O(1)[a]–Zn(1)–N(1)	169.6(2)
		O(1)[a]–Zn(1)–N(2)	89.8(2)
		N(1)–Zn(1)–N(2)	89.3(2)
5			
Co(1)–O(1)	2.012(3)	Co(1)–O(1)–Co(2)	101.99(11)
Co(1)–O(2)	1.938(3)	Co(1)–O(4)–Co(2)	102.04(11)
Co(1)–O(4)	2.081(3)	O(1)–Co(1)–O(2)	121.01(12)
Co(1)–N(1)	2.157(3)	O(1)–Co(1)–O(4)	77.67(10)
Co(1)–N(2)	2.178(3)	O(1)–Co(1)–N(1)	89.29(11)
Co(2)–O(1)	2.070(3)	O(1)–Co(1)–N(2)	131.32(13)
Co(2)–O(4)	1.999(3)	O(2)–Co(1)–O(4)	107.61(11)
Co(2)–O(5)	1.916(3)	O(2)–Co(1)–N(1)	91.25(12)
Co(2)–N(3)	2.172(3)	O(2)–Co(1)–N(2)	107.02(12)
Co(2)–N(4)	2.159(4)	O(4)–Co(1)–N(1)	160.71(12)
Co(1)···Co(2)	3.172(7)	O(4)–Co(1)–N(2)	96.02(12)
		N(1)–Co(1)–N(2)	81.87(13)
		O(1)–Co(2)–O(4)	78.18(10)
		O(1)–Co(2)–O(5)	93.02(11)
		O(1)–Co(2)–N(3)	167.72(12)
		O(1)–Co(2)–N(4)	104.43(13)
		O(4)–Co(2)–O(5)	128.42(13)
		O(4)–Co(2)–N(3)	90.55(12)
		O(4)–Co(2)–N(4)	101.39(13)
		O(5)–Co(2)–N(3)	90.19(12)
		O(5)–Co(2)–N(4)	129.76(14)
		N(3)–Co(2)–N(4)	82.39(14)

[a] Symmetry operators for the generated atoms: $-x$, $-y$, $-z + 1$ for **1**·2$CHCl_3$; $-x + 1$, $-y$, $-z + 2$ for **2**; $-x + 1$, $-y$, $-z + 1$ for **3**; $-x + 2$, $-y$, $-z + 1$ for **4**.

Complexes $[Co^{II}_2(L^1)_2]\cdot 2CHCl_3$ (**1**·2CHCl$_3$), $[Zn^{II}_2(L^1)_2]$ (**2**), $[Co^{II}_2(L^2)_2]$ (**3**), $[Zn^{II}_2(L^2)_2]$ (**4**) and $[Co^{II}_2(L^3)_2]$ (**5**) exhibit closely similar structures. Perspective views of the metal coordination environments of the diphenoxido-bridged dimetal(II) complexes are presented in Figures 1, S3 (Supporting Information), 2, S4 (Supporting Information) and 3. For **1**·2CHCl$_3$, **2**, **3** and **4**, the metal–ligand unit is located on a crystallographically imposed centre of inversion forming the dinuclear structure. For **1**·2CHCl$_3$ and **2**–**5**, the two M^{II} ions are in five-coordinate environments bridged by two phenolato oxygen atoms O1 and O1*/O4 from two $(L^1)^{2-}/(L^2)^{2-}/(L^3)^{2-}$ ligands. The coordination around each M^{II} ion is completed by two nitrogen atoms [pyridine N2 (**1**·2CHCl$_3$, **2**, **3** and **4**) or dimethylamine N2 (**5**) and a tertiary amine N1] and a phenolato oxygen atom O2 provided by a 2-*tert*-butyl-4-methyl/methoxyphenolato ring. Thus, each M^{II} ion is in an N_2O_3 coordination environment. The equatorial plane consists of two phenolato oxygen atoms O(1) and O(2) as well as a pyridine/dimethylamine nitrogen atom N(2), and the axial positions are occupied by a phenolato oxygen atom O(1)*/O4 and a tertiary amine nitrogen atom N(1). For **5**, the equatorial positions around Co(2) are occupied by two phenolato oxygen atoms O(4) and O(5) and an amine nitrogen atom N(4), and the axial positions are provided by a phenolato oxygen atom O(1) and an amine nitrogen atom N(3). The geometry around each M^{II} ion in **1**·2CHCl$_3$, **2**, **3** and **4** is distorted trigonal-bipyramidal [τ = 0.76 (**1**·2CHCl$_3$), 0.77 (**2**), 0.74 (**3**) and 0.76 (**4**); for ideal square-pyramidal geometry τ = 0 and for ideal trigonal-bipyramidal τ = 1].[12] In the case of **5**, the geometry around the two Co^{II} centres is slightly different: Co(1): τ = 0.49; Co(2): τ = 0.63. The M^{II} ions are in the equatorial plane (**1**·2CHCl$_3$) or almost in the plane [displaced towards N(1) by 0.045(3), 0.015(8) and 0.035(2) Å for **2**, **3** and **4**, respectively]. For **5**, the Co(2) ion is out of the equatorial plane towards O(1) by 0.074(4) Å.

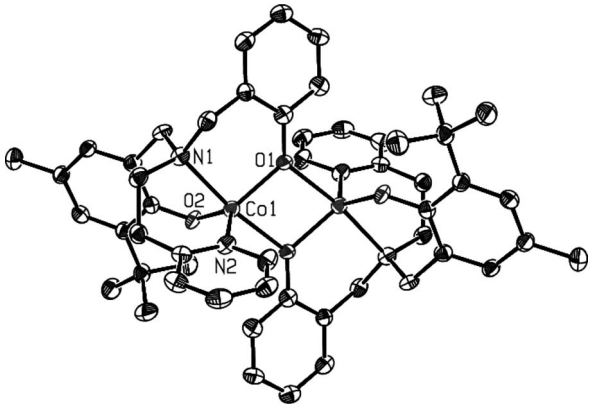

Figure 1. Perspective view of $[Co^{II}_2(L^1)_2]$ in the crystal of $[Co^{II}_2(L^1)_2]\cdot 2CHCl_3$ (**1**·2CHCl$_3$). Only donor atoms are labelled. All hydrogen atoms are excluded for clarity.

The following comments on the trends of metal–ligand bond lengths (Table 1) are in order. For **1**·2CHCl$_3$, **2**, **3** and **4**, the M^{II}–N(pyridine) bonds are consistently shorter (by ca. 0.1 Å) than the M^{II}–N(amine) bonds. Among the two

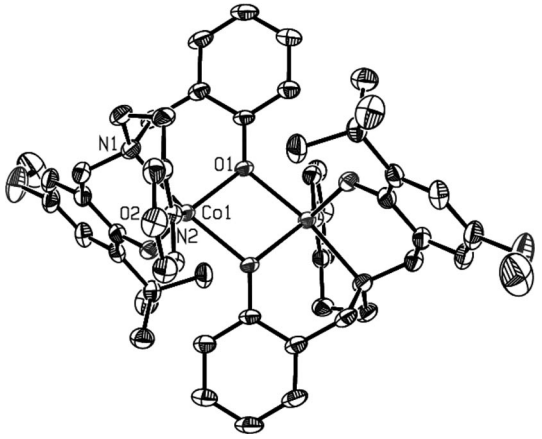

Figure 2. Perspective view of the crystal structure of $[Co^{II}_2(L^2)_2]$ (**3**). Only donor atoms are labelled. All hydrogen atoms are excluded for clarity.

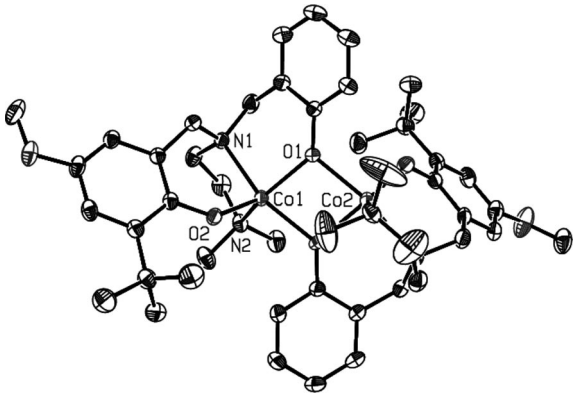

Figure 3. Perspective view of the crystal structure of $[Co^{II}_2(L^3)_2]$ (**5**). Only donor atoms are labelled. All hydrogen atoms are excluded for clarity.

M^{II}–$O_{phenolato}$ bonds in the equatorial plane, the M^{II}(1)–O(2) bonds are shorter (by ca. 0.04 Å) than the M^{II}(1)–O(1) bonds (Table 1), implying that the substituted phenolato ring coordinates more effectively than the unsubstituted phenolato ring. This trend is more pronounced in the case of **5** since, in this case, the two Co^{II}–N distances are closely similar. The M^{II}(1)–O(1)–M^{II}(1)* angles are 100.23(11)° (**1**·2CHCl$_3$), 101.64(13)° (**2**), 101.22(12)° (**3**) and 101.8(2)° (**4**). For **5**, the Co(1)–O(1)–Co(2) and Co(1)–O(4)–Co(2) angles are 101.99(11)° and 102.04(11)°, respectively. The $M^{II}_2O_2$ core in **1**·2CHCl$_3$, **2**, **3** and **4** is planar, as dictated by symmetry. The Co_2O_2 core in **5** is almost planar with a dihedral angle [between the two planes passing through the atoms Co(1)–O(1)–Co(2), and Co(1)–O(4)–Co(2)] of 4.01(12)°. However, the bridge is slightly asymmetric, and the M^{II}(1)–O(1) bonds are shorter (by ca. 0.15 Å) than the M^{II}(1)–O(1)* bonds. The same trend applies to **5**, although the extent of asymmetry is less here (by ca. 0.07 Å). The distances between the two M^{II} centres are as follows: 3.139(7) Å (**1**·2CHCl$_3$),[11,13] 3.226(9) Å (**2**),[8d,11,14] 3.193(9) Å (**3**), 3.203(9) Å (**4**) and 3.172(7) Å (**5**).

Absorption Spectra

The electronic spectra of the Co^{II} complexes **1**, **3** and **5** in CH_2Cl_2 display the characteristic features of a distorted five-coordinate geometry around the Co^{II} ions (Figure S5–S7, Supporting Information). Crystal-field transitions can be observed at 570 nm and also in the 740–760 nm range. A reasonably intense absorption in the 380–390 nm range was assigned to the phenolato-to-Co^{II} charge-transfer transition.[11,15] Intraligand transitions are visible at even higher energies.

Magnetism

In order to extract information about the nature and extent of magnetic exchange interactions between the two metal centres, temperature-dependent (2–300 K) magnetic susceptibility measurements were carried out on powder samples of **1**, **3** and **5**. The temperature dependence of the $\chi_M T$ product for **1**, **3** and **5** is shown in Figure 4. The values of $\chi_M T$ at room temperature are 4.45 (**1**), 4.20 (**3**) and 4.15 (**5**) $cm^3\,K\,mol^{-1}$. They all decrease upon cooling, indicating the existence of antiferromagnetic interactions. A maximum in the susceptibility curve was observed for **5** at 4.5 K (see inset of Figure 4), whereas no such maxima were observed for **1** and **3** above 2.0 K.

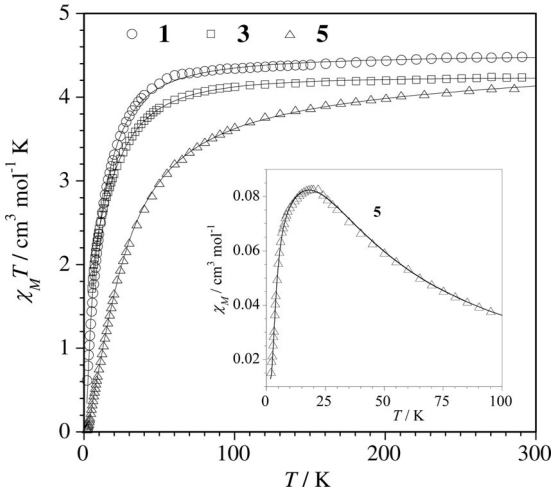

Figure 4. Plot of $\chi_M T$ vs. T for powdered samples of **1**, **3** and **5**. Plot of χ_M vs. T for a powdered sample of **5** shown as inset. The solid lines represent the best theoretical fit, described in the text.

Generally, the ground-state for five-coordinate Co^{II} complexes is a singlet orbital [$^3A_2$ for square-pyramidal (C_{4v}) or trigonal-bipyramidal (C_{3v})], and so no magnetic orbital contribution is expected. In this sense, the spin-only Hamiltonian can be applied for the analysis of magnetic data. Due to the dinuclear nature of **1**, **3** and **5**, the experimental data were modelled by using the Hamiltonian $H = J\hat{S}_1\hat{S}_2 + D(\hat{S}_{z1}^2 + \hat{S}_{z2}^2)$, with $S_1 = S_2 = {}^3/_2$. In order to reduce the number of variables and to avoid over-parameterisation, the values of D (zero-field splitting parameter) and g ($g_z = g_x = g_y$) were considered to be identical for the two metal ions. Satisfactory fits were obtained by using the above Hamiltonian, and the values of the fitting parameters are given in Table 2. The values of the exchange interaction parameters are in agreement with those observed for closely similar compounds.[11,13]

Table 2. Magnetic data fitting (g and D) and distortion (τ)[a] parameters for **1**, **3** and **5**.

Compound	g	D [cm^{-1}]	$-J$ [cm^{-1}]	τ
1	2.20(1)	15.8(2)	1.84(1)	0.76
3	2.15(1)	24.1(2)	1.32(2)	0.74
5	2.12(1)	22.5(2)	5.70(3)	0.49 and 0.63

[a] $\tau = 0$ for ideal square-pyramidal and $\tau = 1$ for ideal trigonal-bipyramidal geometry.

The Co^{II} ions in both symmetries (square-pyramidal and trigonal-bipyramidal) have three magnetic orbitals in common: $d_{x^2-y^2}$, d_{xy}, and d_{z^2}, and the pathway for magnetic exchange is propagated through the bridging phenoxido ligands. For the square-pyramidal environment, the $d_{x^2-y^2}$ orbital is more delocalised over the phenoxido bridge, whereas the same is true of the d_{z^2} orbital in the trigonal-bipyramidal geometry. Therefore, these orbitals are important in transmitting magnetic-exchange interactions. These considerations are displayed in Scheme 2. One can see therein the simplified wave functions describing the magnetic orbitals Ψ_A, Ψ_B and Ψ_C, where ϕ_L is the orbital of the bridge (the participation of the peripheral ligands is neglected, and it is assumed that both the metal orbitals have the same energy). The values of the overlap integrals between the magnetic orbitals u and v ($S_{u,v}$) can be estimated as $S_T = 2S_{A,A'} = 2\langle\psi_A|\psi_{A'}\rangle \propto 2\gamma^2$ and $S_T = 2S_{B,C'} = 2\langle\psi_B|\psi_{C'}\rangle \propto \frac{4\gamma^2}{3}$, for square-pyramidal (Case I in Scheme 2) and trigonal-bipyramidal (Case II in Scheme 2) geometry, respectively (the prime refers to the second magnetic orbital in the dimer).[16]

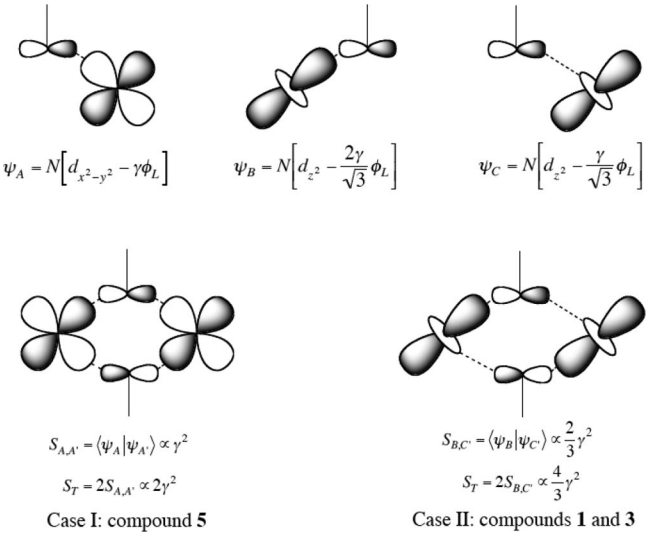

Scheme 2.

In the framework of Kahn's orbital model,[17] it was found that J varies as $S^2_{u,v}$. In this approach, our prediction concerning the relative magnitude of both pathways is expressed by the quotient $\frac{J_{x^2-y^2,x^2-y^2}}{J_{z^2,z^2}} \approx \frac{S^2_{A,A'}}{S^2_{B,C'}} \approx \frac{9}{4}$, showing enhanced magnetic exchange through the $d_{x^2-y^2}$ pathway compared with the d_{z^2} one. It is to be reiterated here that the metal coordination geometry for all the three complexes is in between square-pyramidal and trigonal-bipyramidal (τ = 0.76 for **1** and 0.74 for **3**; τ = 0.49 and 0.63 for **5**). However, compared with the cases of **1** and **3**, the magnetic exchange interaction in **5** will have more involvement of the $d_{x^2-y^2}$ pathway. The observed values of $-J$ for **1** (ca. 1.84) and **3** (ca. 1.32 cm^{-1}) are smaller than that of **5** (ca. 5.70 cm^{-1}), as expected.

Redox Properties

From the standpoint of investigating the potential of the chosen ligands to generate metal-coordinated phenoxyl radical species, the present complexes were examined by cyclic voltammetry. The experiments were performed in CH_2Cl_2 (298 K) at a scan rate of 100 mVs^{-1} by using a platinum working electrode. For **1**, two irreversible oxidative responses at $E_{pa}{}^1$ = 0.62 and $E_{pa}{}^2$ = 0.75 V relative to the SCE (E_{pa} = anodic peak potential) were observed. For **2**, however, a broad (two overlapping irreversible peaks) oxidative response at $E_{pa}{}^1$ = 0.60 and $E_{pa}{}^2$ = 0.74 V relative to the SCE was observed. The cases of **1** and **2** are displayed in Figures S8 and S9 (Supporting Information), respectively. Notably, for **3** and **5** (Figure 5), the responses are well behaved. Two well-resolved quasi-reversible one-electron oxidative responses were observed at $E_{1/2}{}^1$ = 0.40 (ΔE_p = 110 mV) and 0.41 (ΔE_p = 100 mV), and $E_{1/2}{}^2$ = 0.53 (ΔE_p = 100 mV) and 0.52 V (ΔE_p = 100 mV) relative to the SCE, respectively. However, complex **4** displays two successive (not so well-resolved) quasi-reversible one-electron oxidative responses at $E_{1/2}{}^1$ = 0.40 (ΔE_p = 80 mV) and $E_{1/2}{}^2$ = 0.52 V (ΔE_p = 80 mV) relative to the SCE (Figure S10, Supporting Information). We assigned the oxidative responses as being due to successive oxidation of metal-coordinated substituted phenolato groups generating phenoxyl radicals (ligand-centred oxidations; see below). Introduction of the electron-releasing methoxy group at the *p*-position of the phenolato ring in the ligands H_2L^2 and H_2L^3 renders the substituted phenolato ring electron-rich and hence readily oxidised.[1i,7b] The $E_{1/2}$ (or E_{pa}) values for **3**, **4** and **5** are lower than those of **1** and **2**, as expected. Moreover, the nature of the redox response also changes (irreversible nature of the CV response of **1** and **2** changes to quasi-reversible for **3**, **4** and **5**). The effect of replacement of a *p*-methyl group by a *p*-methoxy group is thus quite distinct. Given the fact that the two phenolato ring oxidations occur at the same or at closely similar potentials (see above), we can conclude that in the two Zn^{II} complexes **2** and **4** there is greatly reduced redox communication between the two redox-active phenolato moieties.[6d]

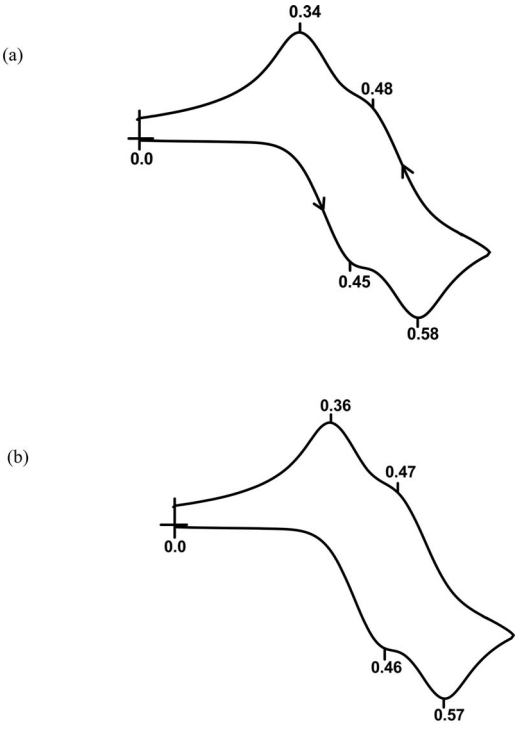

Figure 5. Cyclic voltammograms (100 $mV\,s^{-1}$) of a 1.0 mM solution of (a) **3** and (b) **5** at a platinum electrode in CH_2Cl_2 (0.1 M in TBAP) at 298 K. Indicated potentials (in V) are relative to the SCE.

Electrochemical Generation of Two-Electron Oxidised Species: Characterisation and Stability

Coulometrically generated two-electron oxidised species of **1** and **2** are not stable enough to allow their redox and spectroscopic characterisation. This is understandable, given the irreversible nature of their redox responses (see above).

The two-electron oxidised species of **3**–**5** were generated by controlled-potential electrolysis (298 K) of their CH_2Cl_2 solutions (containing 0.1 M TBAP) [for **3**, applied potential = 0.80 V, n (number of electron transferred) = 2.01, colour change from light pink to greenish brown; for **4**, applied potential = 0.70 V, n = 1.97, colour change from colourless to deep green; for **5**, applied potential = 0.80 V, n = 1.98, colour change from light pink to greenish brown]. The electro-generated two-electron oxidised species of **3**–**5** were stable enough for their CV, absorption and EPR spectra to be recorded. Such solutions of two-electron oxidised species display two successive reductive responses at almost the same potential [the CV scans of oxidised solutions of **3**, **4** and **5** are displayed in Figures S11, S12 and S13 (Supporting Information), respectively]. It is, therefore, logical to assume that there is no gross structural change during the redox process.

The electronic spectra of the two-electron oxidised species of **3**, **4** and **5** [Figure 6 for **3**; Figures S14 and S15 (Supporting Information) for **4** and **5**, respectively] show characteristic absorptions: 430 nm ($\varepsilon \approx 8000\ M^{-1}cm^{-1}$) and 690 nm ($\varepsilon \approx 1250\ M^{-1}cm^{-1}$) for **3**; 405 nm (sh) ($\varepsilon \approx 9500\ M^{-1}cm^{-1}$), 420 nm ($\varepsilon \approx 11500\ M^{-1}cm^{-1}$) and 580 nm ($\varepsilon \approx 2900\ M^{-1}cm^{-1}$)

for **4**; 415 nm ($\varepsilon \approx 8800\ M^{-1}cm^{-1}$) and 760 nm ($\varepsilon \approx 1450\ M^{-1}cm^{-1}$) for **5**. Similar absorptions have previously been observed for metal-coordinated phenoxyl radical species and can be attributed to the π–π* transitions of phenoxyl radicals.[1i,1j,5c,9c,9d]

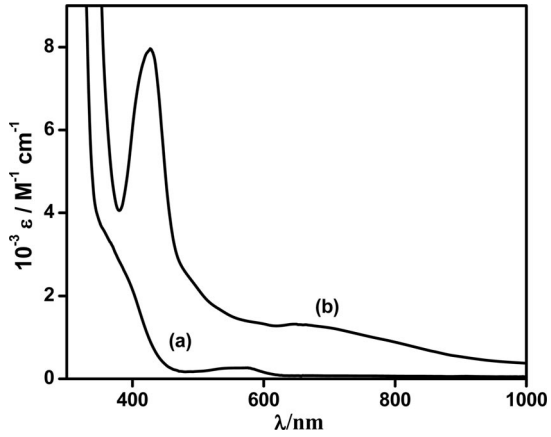

Figure 6. Absorption spectra (CH_2Cl_2; 298 K) of (a) **3** and (b) its coulometrically generated two-electron oxidised species (1 mM; 298 K).

Although the two-electron oxidised species of **3**–**5** are relatively stable in air and at ambient temperature, they gradually decompose by means of first-order kinetics. The k_{decay} of the product of the two-electron oxidations of **3**, **4** and **5** are $2.36 \times 10^{-1}\ min^{-1}$ ($t_{1/2} \approx 2.94$ min), $6.66 \times 10^{-2}\ min^{-1}$ ($t_{1/2} \approx 10.40$ min) and $2.92 \times 10^{-2}\ min^{-1}$ ($t_{1/2} \approx 23.71$ min), respectively. These values are closely similar to those previously reported for metal-coordinated phenoxyl radical species.[6a,7b,10a,10b] A representative case for the time course of spectroscopic change during decay of **5** is displayed in Figure 7. Figures S19 and S20 (Supporting Information) display such a spectroscopic change for **3** and **4**, respectively. From the k_{decay} value, it is evident that the two-electron oxidised species of **5** is the most stable compared with those of **3** and **4**. This can be rationalised if we invoke the effect of the chelate ring size. It is well known that a five-membered chelate-ring-forming ligand provides enhanced electron donation to a metal ion compared with a six-membered chelate-ring-forming ligand.[18] The stability of M^{II}-coordinated phenoxyl radical complexes depends on the donor properties of the equatorial nitrogen atoms[7a,7c] and the binding ability of a particular chelate-ring-forming donor site. With weaker binding to a metal ion, the phenoxyl radical is less stable. In **3** and **4**, the equatorial coordination site is provided by a π-accepting pyridine nitrogen atom, and it is part of a six-membered chelate ring. On the other hand, the equatorial coordination site in **5** is occupied by a σ-donating alkylamine nitrogen atom, which is a part of a five-membered chelate ring. So why the product of the two-electron oxidised species of **5** is more stable than that of **3** (and also **4**) is understandable. The difference in the π–π* transition energy of metal-coordinated phenoxyl radical species observed for the two-electron oxidised species of **3** (430 nm) and **5** (415 nm) justifies our conclusion that $(L^3)^{2-}$ is a stronger ligand than $(L^2)^{2-}$. Although both methyl and methoxy groups are electron-releasing, the stability of the metal-coordinated phenoxyl radical species is enhanced by the presence of a *p*-OMe over a *p*-Me group because of resonance stabilisation. The more electron-donating phenolato ring substituent affords the more stable radical.[1j] Stabilisation of metal-coordinated phenoxyl radical species by a *p*-OMe group, as encountered here, has been observed before.[1i,1j,6a,6b]

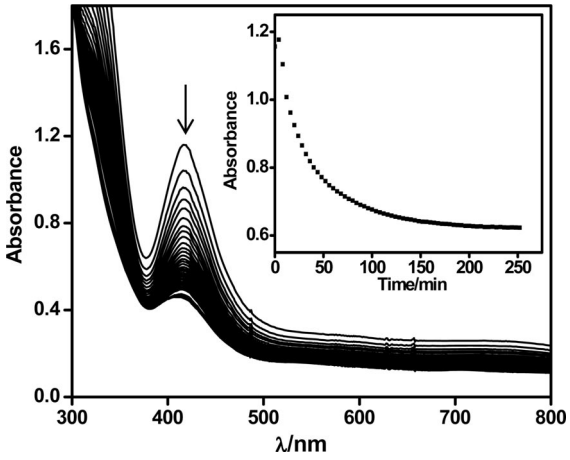

Figure 7. Time course of the spectroscopic change of two-electron coulometrically generated oxidised species of **5** in CH_2Cl_2 containing 0.1 M TBAP (1 mM; 298 K). First-order decay plot shown as inset.

A comparison of the k_{decay} values between the present diphenoxido-bridged Zn^{II} complex **4** [$(L^2)^{2-}$, R = OMe] and that of the corresponding Zn^{II} complex[11] of L^{2-} [H_2L = 2,4-di-*tert*-butyl-6-({(2-hydroxybenzyl)[2-(2-pyridyl)ethyl]-amino}methyl)phenol] with R = *t*Bu is in order. The k_{decay} value ($3.1042 \times 10^{-1}\ min^{-1}$; $t_{1/2} \approx 2.23$ min) for the diphenoxido-bridged Zn^{II} complex of L^{2-} with R = *t*Bu is noteworthy.[11] For the present complex **4** ($k_{decay} = 6.66 \times 10^{-2}\ min^{-1}$; $t_{1/2} \approx 10.40$ min) a substantial increase (about five times) in the stability of the Zn^{II}-coordinated phenoxyl radical species has been observed.

X-band EPR spectra of CH_2Cl_2 solutions of coulometrically generated two-electron oxidised species of **3**, **4** and **5** at 298 K exhibit isotropic signals at g = 2.006, 2.005 and 2.006, respectively [Figure 8 for **3**; Figures S16 and S17 (Supporting Information), for **4** and **5**, respectively]. Moreover, some interesting changes in line widths are evident. Because the MeO-substituted ligand $(L^2)^{2-}$ gives rise to enhanced stability of the two-electron oxidised species compared with its Me-substituted counterpart $(L^1)^{2-}$ (see below) and because the Zn^{II} ion is redox-inactive, we investigated the EPR spectroscopic features of two-electron oxidised species of **4** in reasonable detail. Notably, for **4**, the EPR spectrum recorded at 120 K consists of a five-line symmetric pattern centred at g = 2 (Figure 9). It should be pointed out here that we did not observe a half-field signal at g = 4. Furthermore, the relative intensity of the spectroscopic feature observed varies significantly in its intensity for different preparations. The spectrum was successfully

simulated (Figure 9) by deconvolution into two distinct subspectra by the combination of a spin-triplet resonance (S = 1; subspectrum I) that gives rise to the symmetric split-line pattern that was assigned to the bis(phenoxyl radical)-coordinated dizinc(II) complex and an isotropic S = ½ signal at g = 2 (subspectrum II) corresponding to the (phenolato)-(phenoxyl radical)-coordinated dizinc(II) complex. For simulation of the S = 1 signal, we assumed that the exchange coupling between the two phenoxyl radicals in the bis-(phenoxyl radical)-coordinated dizinc(II) complex is much larger than the Zeeman splitting ($h\nu$ = 0.3 cm^{-1} at the X-band frequency) for which the singlet and triplet states are well separated in energy without any significant level mixing. With this assumption, we could simulate the S = 1 component as an isolated spin triplet with axial zero-field splitting (ZFS), which arises from the combined effect of intramolecular exchange and spin-dipolar couplings of two radical spins.[5d,9d] The parameters are: $g_x = g_y$ = 2.006 and g_z = 2.004, $|D|$ = 0.0068 cm^{-1}, E = 0, $W_x = W_y$ = 15, W_z = 12 G (S = 1); $g_x = g_y = g_z$ = 2.006, $W_x = W_y = W_z$ = 15 G (S = ½). Notably, the simulation is the sum of two subspectra I and II in a 1:3 ratio. Moreover, the intensity of the dominant signal corresponding to the (phenolato)-(phenoxyl radical)-coordinated dizinc(II) complex (S = ½) at $g \approx 2$ and the signal due to a radical marker (the 2,4,6-tri-*tert*-butylphenoxyl radical)[19] are comparable (Figure S18, Supporting Information) under identical experimental conditions (concentration of **4** and radical marker: 1 mM in CH_2Cl_2; invariant machine setup). The formation of the (phenolato)(phenoxyl radical)-coordinated dizinc(II) complex (S = ½) from the comproportionation reaction between the "bis(phenolato)dizinc(II)" and "bis(phenoxyl radical)-coordinated dizinc(II)" species is justified, given the redox potential values of the two relevant redox processes: (phenolato)(phenoxyl radical)-coordinated dizinc(II)/bis(phenolato)dizinc(II) (0.40 V) and bis(phenoxyl radical)-coordinated dizinc(II)/(phenolato)(phenoxyl radical)-coordinated dizinc(II) (0.52 V). A similar behaviour was observed before.[5d,9d]

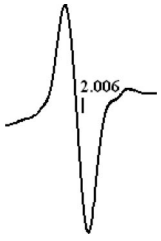

Figure 8. X-band EPR spectrum (CH_2Cl_2; 298 K) of the coulometrically generated two-electron oxidised species of **3** (1 mM; 298 K).

Complexes **3** and **5** are EPR-silent (S = 0) due to antiferromagnetic exchange coupling between the two Co^{II} centres mediated by the diphenoxido bridge (see above). For two-electron oxidised species of the dicobalt(II) complexes **3** and **5**, the EPR spectroscopic feature at 298 K (isotropic signal at g = 2) is closely similar to that of **4**. Efforts are underway to investigate the EPR spectroscopic feature of **3** and **5** at low temperature. Understandably, for paramagnetic Co^{II} complexes, the interaction between d electrons and the phenoxyl radical is expected to be complex.[9d] Due to lack of EPR spectroscopic results for **3** and **5** at low temperature being available, we decided to extract information about the effective magnetic moment values of **5** in CH_2Cl_2 (296 K) and its two-electron coulometrically oxidised solutions (1 mM in CH_2Cl_2, containing 0.1 M TBAP; 298 K), and solution-state magnetic susceptibility measurements were carried out. The μ_{eff} values per metal atom are 3.92 μ_B (solid-state value: 4.07 μ_B at 300 K; see above) and 4.85 μ_B. Future endeavours will focus on justifying the observed μ_{eff} values along with low-temperature EPR spectroscopic results. From the available spectroscopic results of the two-electron oxidised species of **3**–**5**, it is clear that the observed redox responses are due to M^{II}-coordinated (M = Co, Zn) ligand-centred oxidation (metal-coordinated phenolato to metal-coordinated phenoxyl radical).

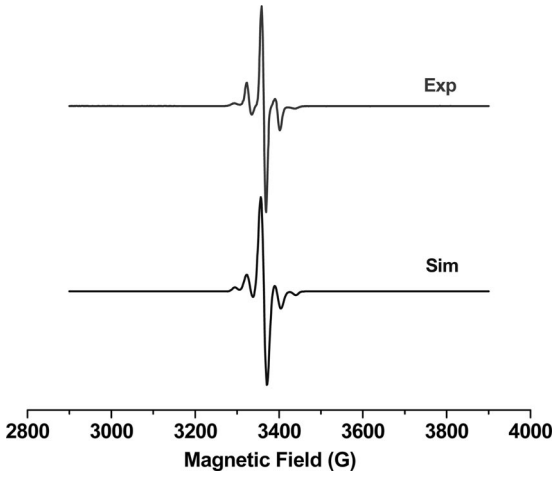

Figure 9. Upper trace: X-band EPR spectrum (120 K; ν = 9.445 GHz; power = 0.201 mW; receiver gain = 1×10^3; modulation frequency = 100 kHz; modulation amplitude = 10 G) recorded for the two-electron coulometrically oxidised complex **4** (1 mM) in CH_2Cl_2 (0.1 M in TBAP). Lower trace: simulated EPR spectrum. Simulation parameters are described in the text.

Computational Results

To extract information about the site of oxidation, single-point DFT calculations at the B3LYP level of theory were performed on all five complexes by using their X-ray crystallographic coordinates. By analysing the nature of the HOMO in each case, it appears that it is a predominantly ligand-based orbital, and there is very little contribution from the metal centre. The maximum contribution comes from the substituted phenolato ring of the ligand, and the HOMO is mainly delocalised over the substituted phenol ring of the ligand with the contribution from the phenolic oxygen atom. The contour plots of the HOMO for **1**–**5** are in Figures 10, 11 and S21–S24 (Supporting Information), respectively. Quantitative evaluations of the atomic orbital contributions to the relevant HOMOs and the energy of the HOMOs are summarised in Table 3.

Table 3. Results of DFT calculations.

Complexes	Energy of HOMO [kcal/mol]	Composition of HOMO Contribution (%) from substituted[a] phenolato ring	Total contribution (%) from ligand	Contribution (%) from metal ion
$[Co^{II}_2(L^1)_2]$ (**1**)	–102.33	60	94	5
$[Zn^{II}_2(L^1)_2]$ (**2**)	–99.78	62	96	3
$[Co^{II}_2(L^2)_2]$ (**3**)	–101.45	66	95	4
$[Zn^{II}_2(L^2)_2]$ (**4**)	–99.78	64	96	3
$[Co^{II}_2(L^3)_2]$ (**5**)	–97.80	66	95	4

[a] 2-*tert*-Butyl-4-methyl unit for **1** and **2**; 2-*tert*-butyl-4-methoxy unit for **3**, **4**, and **5**.

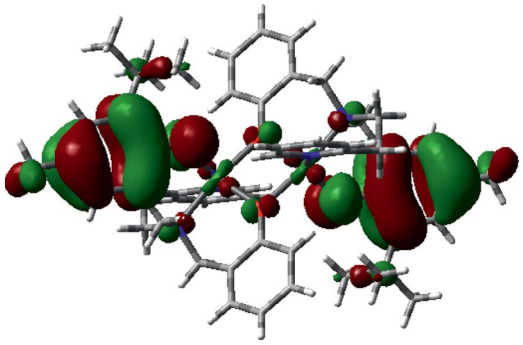

Figure 10. Contour plot of the HOMO of **1**.

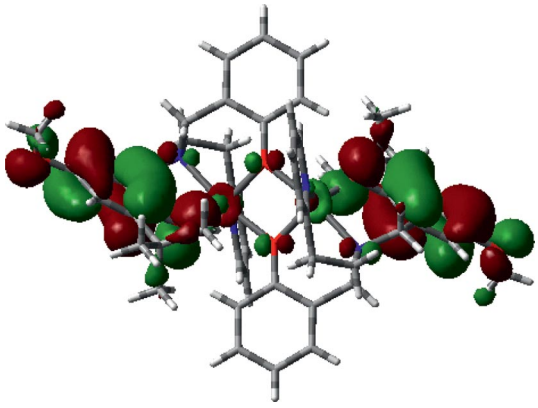

Figure 11. Contour plot of the HOMO of **3**.

Summary and Concluding Remarks

From the viewpoint of the properties of metal-coordinated phenoxyl radical species, we have extended our previous studies in this work[11] and successfully synthesised and characterised a class of dinuclear cobalt(II) and zinc(II) complexes with new tripodal ligands [varying the donor properties by the electron-releasing substituents (methoxy and methyl)] providing N_2O_2 donor sites and containing two different types of phenol ring (one substituted and the other one unsubstituted). The metal ions in these complexes are between square-pyramidal and trigonal-bipyramidal in their geometry. The successful preparation and systematic investigation of properties of five closely similar complexes provide a valuable source of information for the understanding of their structures, magnetic properties, redox behaviour (ligand-centred oxidation) and the stability of the metal-coordinated phenoxyl radical species. The composition of the HOMOs of all the complexes (DFT calculations at the B3LYP level of theory) reveals that the oxidation takes place on the substituted phenol ring. The present study provides information about the nature and variation of the redox potential (formation of metal-coordinated phenoxyl radical species) as a function of the electronic effect of the substituent at the *p*-position of the phenolato ring and also gives information on the effect of chelate ring size on the stability of the phenoxyl radical species of the Co^{II}/Zn^{II}-coordinated phenoxyl radicals. Studies on the metal-coordinated phenoxyl radical species in a mononuclear metal coordination environment, which is of more relevance to the galactose oxidase active site, are in progress in our laboratory.

Experimental Section

Material and Reagents: All reagents were obtained from commercial sources and used as received. Solvents were dried/purified as reported previously.[20] The precursors 2-({[2-(2-pyridinyl)ethyl]amino}methyl)phenol[21] for the synthesis of H_2L^1 and H_2L^2 and 2-({[2-(dimethylamino)ethyl]amino}methyl)phenol[22] for the synthesis of H_2L^3 were prepared according to literature procedures. The 2,4,6-tri-*tert*-butylphenoxyl radical was prepared according to a reported procedure.[19] Tetra-*n*-butylammonium perchlorate (TBAP) was prepared and purified as before.[20a] Zinc(II) perchlorate hexahydrate was prepared from the reaction between $ZnCO_3$ and aqueous $HClO_4$.

Syntheses of Ligands

2-*tert*-Butyl-6-({(2-hydroxybenzyl)[2-(2-pyridyl)ethyl]amino}methyl)-4-methylphenol (H_2L^1): The ligand H_2L^1 was prepared by a modification of the method reported by Williams et al.[23] A mixture of 2-({[2-(2-pyridinyl)ethyl]amino}methyl)phenol (2.0 g, 8.77 mmol), 2-*tert*-butyl-4-methylphenol (1.44 g, 8.77 mmol) and paraformaldehyde (0.34 g, 11.40 mmol) was prepared in dry C_2H_5OH (15 mL) and heated to reflux under nitrogen for 16 h. After cooling to room temperature, the pH of the solution was brought to 2 by dropwise addition of HBr (48% aqueous solution), and the solvent was removed under reduced pressure. The resultant yellow oil was dissolved in water (50 mL) and extracted with CH_2Cl_2 (4× 10 mL). The aqueous layer was neutralised with saturated $NaHCO_3$ solution and further extracted with CH_2Cl_2 (4× 10 mL). This organic layer was then washed with saturated brine solution (2× 20 mL) and dried with anhydrous Na_2SO_4. Finally, the solvent was removed under reduced pressure to give a white solid of H_2L^1 (yield: 2.12 g, ca. 60%). $C_{26}H_{32}N_2O_2$ (404): calcd. C 77.23, H 7.92, N 6.93; found C 76.82, H 8.02, N 6.98. ^1H NMR ($CDCl_3$; 80 MHz): δ = 8.69 (d, $J_{H,H}$ = 7.71 Hz, 1 H, $H^{6'}$ of py), 6.76–7.43 (m, 9 H, $H^{3',4',5'}$ of py, $H^{3,5}$ of C_6H_2OH, $H^{3'',4'',5'',6''}$ of C_6H_4OH), 3.96 (s, 4 H, CH_2), 3.29 (t, $J_{H,H}$ = 8.11 Hz, 4 H, CH_2CH_2), 2.30 (s, 3 H, CH_3), 1.40 (s, 9 H, *tert*-butyl) ppm.

2-*tert*-Butyl-6-({(2-hydroxybenzyl)[2-(2-pyridyl)ethyl]amino}methyl)-4-methoxyphenol (H_2L^2): This was prepared in a similar manner to H_2L^1 [2-*tert*-butyl-4-methoxyphenol (1.58 g, 8.77 mmol) was used instead of 2-*tert*-butyl-4-methylphenol] and isolated in 64% yield. $C_{26}H_{32}N_2O_3$ (420): calcd. C 74.29, H 7.62, N 6.67; found C 74.42, H 7.84, N 6.78. ^{1}H NMR ($CDCl_3$; 80 MHz): δ = 9.20 (d, $J_{H,H}$ = 7.64 Hz, 1 H, H$^{6'}$ of py), 6.93–7.86 (m, 9 H, H$^{3',4',5'}$ of py, H^{3,5} of C_6H_2OH, H$^{3'',4'',5'',6''}$ of C_6H_4OH), 4.26 (s, 3 H, OCH_3), 4.00 (s, 4 H, CH_2), 3.33 (t, $J_{H,H}$ = 8.23 Hz, 4 H, CH_2CH_2), 1.36 (s, 9 H, *tert*-butyl) ppm.

2-*tert*-Butyl-6-({[2-(dimethylamino)ethyl](2-hydroxybenzyl)amino}-methyl)-4-methoxyphenol (H_2L^3): This was prepared in a similar manner to H_2L^1 [2-({[2-(dimethylamino)ethyl]amino}methyl)-phenol (1.70 g, 8.77 mmol) was used instead of 2-({[2-(2-pyridinyl)-ethyl]amino}methyl)phenol] and isolated in 71% yield. $C_{23}H_{34}N_2O_3$ (386): calcd. C 71.50, H 8.81, N 7.25; found C 70.92, H 8.92, N 6.96. ^{1}H NMR ($CDCl_3$; 80 MHz): δ = 7.23–7.86 (m, 6 H, H^{3,5} of C_6H_2OH, H$^{3',4',5',6'}$ of C_6H_4OH), 4.10 (s, 3 H, OCH_3), 4.03 (s, 4 H, CH_2), 3.13 (t, $J_{H,H}$ = 8.19 Hz, 4 H, CH_2CH_2), 2.83 [s, 6 H, $N(CH_3)_2$], 1.40 (s, 9 H, *tert*-butyl) ppm.

Syntheses of Complexes

$[Co^{II}_2(L^1)_2]$ (1): To a magnetically stirred mixture of H_2L^1 (0.15 g, 0.371 mmol) and Et_3N (0.075 g, 0.742 mmol) in CH_3OH (7 mL) was added a solution of $Co(OAc)_2{\cdot}4H_2O$ (0.092 g, 0.371 mmol) in CH_3OH (7 mL) dropwise, and the resultant mixture was heated to reflux for 2 h. The pink precipitate that formed was collected by filtration, washed with CH_3OH and dried in vacuo (yield: 0.195 g, ca. 61%). The complex was recrystallised by diffusion of *n*-hexane into a concentrated solution of the complex in $CHCl_3/CH_3OH$ (3:1, v/v) to afford pink crystals with two molecules of $CHCl_3$ as the solvent of crystallisation {$[Co^{II}_2(L^1)_2]{\cdot}2CHCl_3$ (**1**·2$CHCl_3$)}. Such crystals were suitable for an X-ray structural study. $C_{52}H_{60}Co_2N_4O_4$ (921.86): calcd. C 67.69, H 6.51, N 6.07; found C 67.62, H 6.48, N 6.11. IR (KBr, selected peak): $\tilde{\nu}$ = 1265 [ν(C–O) of phenolato group] cm^{-1}. UV/Vis (CH_2Cl_2): λ (ε) = 290 (20000), 390 (sh) (2500), 530 (sh) (170), 570 (200), 740 (30 M^{-1}cm^{-1}) nm.

$[Zn^{II}_2(L^1)_2]$ (2): To a magnetically stirred mixture of H_2L^1 (0.1 g, 0.247 mmol) and Et_3N (0.05 g, 0.494 mmol) in CH_3OH (5 mL) was added dropwise a solution of $[Zn(H_2O)_6][ClO_4]_2$ (0.092 g, 0.247 mmol) in CH_3OH (5 mL). The resultant solution was stirred for 1 h. The white precipitate that formed was collected by filtration, washed with CH_3OH and dried in vacuo (yield: 0.144 g, ca. 67%). The complex was recrystallised by diffusion of *n*-hexane into a concentrated solution of the complex in $CHCl_3/CH_2Cl_2$ (1:1, v/v). The white crystals obtained were found to be suitable for an X-ray structural study. $C_{52}H_{60}N_4O_4Zn_2$ (934.78): calcd. C 66.75, H 6.42, N 6.00; found C 66.71, H 6.45, N 6.06. IR (KBr, selected peak): $\tilde{\nu}$ = 1267 [ν(C–O) of phenolato group] cm^{-1}. ^{1}H NMR (400 MHz, $CDCl_3$): δ = 8.81 (s, 1 H, H$^{6'}$ of py), 7.64 (t, $J_{H,H}$ = 7.34 Hz, 1 H, H$^{4'}$ of py), 7.26 (s, 2 H, H^{3,5} of *t*BuC_6H_2O), 7.10 (d, $J_{H,H}$ = 7.61 Hz, 1 H, H$^{3'}$ of py), 6.96 (t, $J_{H,H}$ = 7.57 Hz, 2 H, H$^{5'}$ of py, H$^{4''}$ of C_6H_4O), 6.91 (d, $J_{H,H}$ = 7.03 Hz, 1 H, H$^{6''}$ of C_6H_4O), 6.68 (d, $J_{H,H}$ = 7.04 Hz, 1 H, H$^{3''}$ of C_6H_4O), 6.51 (t, $J_{H,H}$ = 7.14 Hz, 1 H, H$^{5''}$ of C_6H_4O), 3.18 (s, 4 H, CH_2), 2.99 (m, 2 H, CH_2CH_2), 2.78 (m, 2 H, CH_2CH_2), 2.17 (s, 3 H, CH_3), 1.25 (s, 9 H, *tert*-butyl) ppm.

$[Co^{II}_2(L^2)_2]$ (3): Complex **3** was synthesised from H_2L^2 (0.1 g, 0.238 mmol) and $Co(OAc)_2{\cdot}4H_2O$ (0.059 g, 0.238 mmol) in CH_3OH (12 mL) by the same procedure as described for **1** (yield: 0.148 g, ca. 65%). Pink crystals suitable for an X-ray structural study were obtained by diffusion of diethyl ether into a concentrated solution of the complex in CH_2Cl_2. $C_{52}H_{60}Co_2N_4O_6$ (953.86): calcd. C 65.42, H 6.29, N 5.87; found C 65.57, H 6.20, N 5.71. IR (KBr, selected peak): $\tilde{\nu}$ = 1270 [ν(C–O) of phenolato group] cm^{-1}. UV/Vis (CH_2Cl_2): λ (ε) = 290 (20500), 310 (18500), 390 (sh) (3000), 570 (220), 760 (35 M^{-1}cm^{-1}) nm.

$[Zn^{II}_2(L^2)_2]$ (4): Complex **4** was synthesised from H_2L^2 (0.15 g, 0.357 mmol) and $[Zn(H_2O)_6][ClO_4]_2$ (0.133 g, 0.357 mmol) in CH_3OH (14 mL) by the same procedure as described for **2** (yield: 0.214 g, ca. 62%). White crystals suitable for an X-ray structural study were obtained by slow concentration of a solution of the complex in a CH_2Cl_2/*n*-hexane mixture. $C_{52}H_{60}N_4O_6Zn_2$ (966.78): calcd. C 64.54, H 6.21, N 5.79; found C 64.68, H 6.34, N 5.67. IR (KBr, selected peak): $\tilde{\nu}$ = 1271 [ν(C–O) of phenolato group] cm^{-1}. ^{1}H NMR (400 MHz. $CDCl_3$): δ = 8.84 (s, 1 H, H$^{6'}$ of py), 7.63 (t, $J_{H,H}$ = 7.70 Hz, 1 H, H$^{4'}$ of py), 7.26 (s, 2 H, H^{3,5} of *t*BuC_6H_2O), 7.09 (d, $J_{H,H}$ = 7.56 Hz, 1 H, H$^{3'}$ of py), 6.93 (t, $J_{H,H}$ = 7.08 Hz, 2 H, H$^{5'}$ of py, H$^{4''}$ of C_6H_4O), 6.81 (d, $J_{H,H}$ = 7.01 Hz, 1 H, H$^{6''}$ of C_6H_4O), 6.52 (d, $J_{H,H}$ = 7.12 Hz, 1 H, H$^{3''}$ of C_6H_4O), 6.48 (t, $J_{H,H}$ = 7.06 Hz, 1 H, H$^{5''}$ of C_6H_4O), 3.74 (s, 3 H, OCH_3), 3.47 (s, 4 H, CH_2), 3.03 (m, 2 H, CH_2CH_2), 2.77 (m, 2 H, CH_2CH_2), 1.21 (s, 9 H, *tert*-butyl) ppm.

$[Co^{II}_2(L^3)_2]$ (5): Complex **5** was synthesised from H_2L^3 (0.15 g, 0.389 mmol) and $Co(OAc)_2{\cdot}4H_2O$ (0.097 g, 0.389 mmol) in CH_3OH (14 mL) by the same procedure as described for **1** (yield: 0.207 g, ca. 60%). Pink crystals suitable for X-ray structural study were obtained by diffusion of *n*-hexane into a concentrated solution of the complex in $CHCl_3$. $C_{46}H_{64}Co_2N_4O_6$ (885.86): calcd. C 62.31, H 7.22, N 6.32; found C 62.42, H 7.34, N 6.41. IR (KBr, selected peak): $\tilde{\nu}$ = 1265 [ν(C–O) of phenolato group] cm^{-1}. UV/Vis (CH_2Cl_2): λ (ε) = 290 (18500), 310 (17000), 380 (sh) (2000), 570 (260), 750 (40 M^{-1}cm^{-1}) nm.

Physical Measurements: Elemental analyses were obtained with a Thermo Quest EA 1110 CHNS-O instrument, Italy. Spectroscopic measurements were made with the following instruments: IR (KBr, 4000–600 cm^{-1}): Bruker Vector 22; UV/Vis: Perkin–Elmer Lambda 2 and Agilent 8453 diode-array spectrophotometers. ^{1}H NMR spectra ($CDCl_3$ solution) were obtained with either a Bruker WP-80 (80 MHz) or a JEOL JNM LA (400 MHz) spectrophotometer. Chemical shifts are reported in ppm referenced to TMS. X-band EPR spectra were recorded with a Bruker EMX 1444 EPR spectrometer operating at 9.455 GHz. The EPR spectra were calibrated with diphenylpicrylhydrazyl (DPPH; g = 2.0037). Variable-temperature magnetic susceptibility measurements on polycrystalline samples of **1**, **3** and **5** were performed with a Quantum Design (Model MPMSXL-5) SQUID magnetic susceptometer at Valéncia, Spain. Magnetic susceptibility measurements in MeCN solution were obtained by the Evans' method[24] with a JEOL JNM LA (400 MHz) NMR spectrometer. Susceptibilities were corrected for diamagnetic contributions. Cyclic voltammetric (CV) experiments were performed at 298 K with a CH instruments, electrochemical analyser/workstation model 600B series. The cell contained a Beckman (M 39273) platinum inlay working electrode, a Pt wire auxiliary electrode and a saturated calomel electrode (SCE) as the reference electrode. Details of the cell configuration are as described before.[25] For coulometry, a platinum wire gauze was used as the working electrode. The solutions were ca. 1.0 mM for the complex and 0.1 M for the supporting electrolyte (TBAP).

Crystal Structure Determination: Single crystals of suitable dimensions were used for data collection. Diffraction intensities were collected with a Bruker SMART APEX CCD diffractometer with graphite-monochromated Mo-K_α (λ = 0.71073 Å) radiation at 100(2) K. The data were corrected for absorption. The structures were solved with SIR-97 expanded by Fourier difference syntheses

Table 4. Data collection and structure refinement parameters for **1**·2$CHCl_3$, **2**, **3**, **4**, and **5**.

	1·2$CHCl_3$	**2**	**3**	**4**	**5**
Empiricalformula	$C_{54}H_{62}Cl_6Co_2N_4O_4$	$C_{52}H_{60}N_4O_4Zn_2$	$C_{52}H_{60}Co_2N_4O_6$	$C_{52}H_{60}N_4O_6Zn_2$	$C_{46}H_{64}Co_2N_4O_6$
Formula mass	1161.64	935.78	954.90	967.78	886.87
Temperature [K]	100(2)	100(2)	100(2)	100(2)	100(2)
Radiation (λ [Å])	Mo-K_α (0.71069)	Mo-K_α (0.71069)	Mo-K_α (0.71069)	Mo-K_α (0.71069)	Mo-K_α (0.71069)
Crystal system	monoclinic	monoclinic	monoclinic	monoclinic	monoclinic
Space group (no.)	$P2_1/n$ (14)	$P2_1/n$ (14)	$P2_1/c$ (14)	$P2_1/c$ (14)	$P2_1/n$ (14)
a [Å]	10.116(5)	11.675(5)	12.098(5)	12.061(5)	11.552(5)
b [Å]	16.038(5)	12.901(5)	12.940(5)	13.030(5)	18.660(5)
c [Å]	16.862(5)	15.607(5)	16.090(5)	16.102(5)	21.255(5)
α [°]	90	90	90	90	90
β [°]	91.513(5)	111.292(5)	111.613(5)	111.840(5)	98.610(5)
γ [°]	90	90	90	90	90
V [Å^3]	2734.7(18)	2190.3(14)	2341.8(15)	2348.9(15)	4530(3)
Z	2	2	2	2	4
$D_{calcd.}$ [g cm^{-3}]	1.411	1.419	1.354	1.368	1.300
μ [mm^{-1}]	0.948	1.147	0.763	1.075	0.783
F(000)	1204	984	1004	4576	1880
Crystal size [mm]	0.2 × 0.1 × 0.1	0.2 × 0.1 × 0.1	0.2 × 0.2 × 0.1	0.2 × 0.1 × 0.1	0.2 × 0.2 × 0.1
Unique reflections	6755	5420	5806	5690	11265
R_{int}	0.0586	0.0486	0.0675	0.2232	0.0583
Reflections used [$I > 2\sigma(I)$]	4457	3754	3415	1988	7017
Reflections measured	17965	14246	15257	14274	29891
Goodness-of-fit on F^2	1.067	0.995	0.939	1.049	1.044
Final R indices [$I > 2\sigma(I)$][a,b]	0.0707	0.0630	0.0781	0.0801	0.0715
	0.1654	0.1683	0.1738	0.1562	0.1623
R indices (all data)[a,b]	0.1140	0.0984	0.1422	0.1960	0.1224
	(0.2044)	(0.2325)	(0.2105)	(0.2185)	(0.1970)

[a] $R_1 = \Sigma(|F_o| - |F_c|)/\Sigma|F_o|$. [b] $wR_2 = \{\Sigma[w(|F_o|^2 - |F_c|^2)^2]/\Sigma[w(|F_o|^2)^2]\}^{1/2}$.

and refined with the SHELXL-97 package incorporated in the WinGX 1.64 crystallographic package.[26] The positions of the hydrogen atoms were calculated by assuming ideal geometries, but they were not refined except the hydrogen atom of the solvent molecule $CHCl_3$ in **1**·2$CHCl_3$. All non-hydrogen atoms were refined with anisotropic thermal parameters by full-matrix least-squares procedures on F^2. For **1**·2$CHCl_3$, after anisotropic refinement, unassigned electron density peaks of 1.42 e Å^{-3} and 1.10 e Å^{-3}, and for **5** a peak of 1.21 e Å^{-3} were found in the final difference Fourier map, which may be due to the poor quality of the crystal chosen for data collection. The R_{int} value of **4** is quite high (0.2232), which may be because of the poor quality of the crystal selected for data collection. Unfortunately, we could not grow single crystals of **1**·2$CHCl_3$, **4** and **5** that were any better than the ones used for the present study. Pertinent crystallographic parameters are summarised in Table 4. CCDC-738914 to -738918 (for **1**·2$CHCl_3$ and **2**–**5**, respectively) contain the supplementary crystallographic data. These data can be obtained free of charge from the Cambridge Crystallographic Data Centre via www.ccdc.cam.ac.uk/data_request/cif.

Theoretical Studies: Calculations were performed by using Density Functional Theory (DFT) with Becke's three-parameter hybrid exchange functional[27] and the Lee–Yang–Parr correlation functional (B3LYP).[28] The atomic coordinates of all the complexes were taken from their X-ray structures. The double-ζ basis set of Hay and Wadt (LanL2DZ) was used for metal centres. The ligands' H, C, N and O atoms were described by using the 6-31G-(d) basis sets. All calculations were performed with the Gaussian 03 (G03) suite of programs.[29] Orbital diagrams were generated at an isosurface of 0.02 by using Gaussview 3.0.[30]

Supporting Information (see also the footnote on the first page of this article): ^{1}H NMR spectra of **2** and **4** (Figures S1 and S2, respectively), molecular structures of [$Zn^{II}_2(L^1)_2$] (**2**) and [$Zn^{II}_2(L^2)_2$] (**4**) (Figure S3 and S4, respectively), electronic spectra of Co^{II} complexes **1**, **3** and **5** in CH_2Cl_2 (Figure S5–S7, respectively), CV scans of **1**, **2** and **4** (Figures S8–S10, respectively), CV scans of two-electron oxidised species of **3**, **4** and **5** (Figures S11–S13, respectively), electronic spectra of two-electron oxidised species of **4** and **5** (Figure S14 and S15, respectively), EPR spectrum of two-electron oxidised species of **4** and **5** (Figure S16 and S17, respectively), comparative EPR spectra of the coulometrically generated two-electron oxidised complex **4** and 2,4,6-tri-*tert*-butylphenoxyl radical (Figure S18), decay curve for the two-electron oxidised species of **3** and **4** (Figures S19 and S20, respectively), contour plots of the HOMOs for **2**–**5** (Figures S21–S24, respectively).

Acknowledgments

This work was supported by grants from the Department of Science and Technology (DST), Government of India, New Delhi. R. M. sincerely thanks DST for a J. C. Bose fellowship. We sincerely thank Suman K. Barman for recording and simulating the EPR spectra. We also thank Prof. Dr. Fabrice Thomas (Université Joseph Fourier, Grenoble, France) and Dr. Himanshu Arora for their help in EPR simulation. Comments of the reviewers were very helpful at the revision stage.

[1] a) J. P. Klinman, *Chem. Rev.* **1996**, *96*, 2541–2561; b) J. Stubbe, W. A. van der Donk, *Chem. Rev.* **1998**, *98*, 705–762; c) H. J. Krüger, *Angew. Chem. Int. Ed.* **1999**, *38*, 627–631; d) S. Itoh, M. Taki, S. Fukuzumi, *Coord. Chem. Rev.* **2000**, *198*, 3–20; e) J.-L. Pierre, *Chem. Soc. Rev.* **2000**, *29*, 251–257; f) B. A. Jazdzewski, W. B. Tolman, *Coord. Chem. Rev.* **2000**, *200–202*, 633–685; g) P. Chaudhuri, K. Wieghardt, *Prog. Inorg. Chem.* **2001**, *50*, 151–216; h) J. W. Whittaker, *Chem. Rev.* **2003**, *103*, 2347–2363; i) W. B. Tolman, in *Comprehensive Coordination Chemistry II: From Biology to Nanotechnology* (Eds.: J. A.

McCleverty, T. J. Meyer), Elsevier/Pergamon, Amsterdam, **2004**, vol. 8 (Ed.: L. Que Jr., W. B. Tolman), pp. 715–737; j) F. Thomas, *Eur. J. Inorg. Chem.* **2007**, 2379–2404.
[2] J. Stubbe, *Chem. Commun.* **2003**, 2511–2513.
[3] C. Limberg, *Angew. Chem. Int. Ed.* **2003**, *42*, 5932–5954.
[4] a) Y. Wang, T. D. P. Stack, *J. Am. Chem. Soc.* **1996**, *118*, 13097–13098; b) Y. Wang, J. L. DuBois, B. Hedman, K. O. Hodgson, T. D. P. Stack, *Science* **1998**, *279*, 537–540; c) T. Storr, E. C. Wasinger, R. C. Pratt, T. D. P. Stack, *Angew. Chem. Int. Ed.* **2007**, *46*, 5198–5201; d) T. Storr, P. Verma, R. C. Pratt, E. C. Wasinger, Y. Shimazaki, T. D. P. Stack, *J. Am. Chem. Soc.* **2008**, *130*, 15448–15459.
[5] a) B. Adam, E. Bill, E. Bothe, B. Goerdt, G. Haselhorst, K. Hildenbrand, A. Sokolowski, S. Steenken, T. Weyhermüller, K. Wieghardt, *Chem. Eur. J.* **1997**, *3*, 308–319; b) A. Sokolowski, B. Adam, T. Weyhermüller, A. Kikuchi, K. Hildenbrand, R. Schnepf, P. Hildebrandt, E. Bill, K. Wieghardt, *Inorg. Chem.* **1997**, *36*, 3702–3710; c) A. Sokolowski, J. Müller, T. Weyhermüller, R. Schnepf, P. Hildebrandt, K. Hildenbrand, E. Bothe, K. Wieghardt, *J. Am. Chem. Soc.* **1997**, *119*, 8889–8900; d) E. Bill, J. Müller, T. Weyhermüller, K. Wieghardt, *Inorg. Chem.* **1999**, *38*, 5795–5802; e) P. Chaudhuri, M. Hess, J. Müller, K. Hildenbrand, E. Bill, T. Weyhermüller, K. Wieghardt, *J. Am. Chem. Soc.* **1999**, *121*, 9599–9610; f) T. Kruse, T. Weyhermüller, K. Wieghardt, *Inorg. Chim. Acta* **2002**, *331*, 81–89.
[6] a) A. Philibert, F. Thomas, C. Philouze, S. Hamman, E. Saint-Aman, J.-L. Pierre, *Chem. Eur. J.* **2003**, *9*, 3803–3812; b) F. Michel, F. Thomas, S. Hamman, E. Saint-Aman, C. Bucher, J.-L. Pierre, *Chem. Eur. J.* **2004**, *10*, 4115–4125; c) F. Michel, F. Thomas, S. Hamman, C. Philouze, E. Saint-Aman, J.-L. Pierre, *Eur. J. Inorg. Chem.* **2006**, 3684–3696; d) O. Rotthaus, O. Jarjayes, F. Thomas, C. Philouze, E. Saint-Aman, J.-L. Pierre, *Dalton Trans.* **2007**, 889–895; e) O. Rotthaus, O. Jarjayes, C. Philouze, C. P. D. Valle, F. Thomas, *Dalton Trans.* **2009**, 1792–1800.
[7] a) Y. Shimazaki, S. Huth, S. Hirota, O. Yamauchi, *Bull. Chem. Soc. Jpn.* **2000**, *73*, 1187–1195; b) Y. Shimazaki, S. Huth, S. Hirota, O. Yamauchi, *Inorg. Chim. Acta* **2002**, *331*, 168–170; c) Y. Shimizaki, S. Huth, S. Karasawa, S. Hirota, Y. Naruta, O. Yamauchi, *Inorg. Chem.* **2004**, *43*, 7816–7822; d) Y. Shimazaki, R. Kabe, S. Huth, F. Tani, Y. Naruta, O. Yamauchi, *Inorg. Chem.* **2007**, *46*, 6083–6090; e) Y. Shimazaki, T. Yajima, T. Shiraiwa, O. Yamauchi, *Inorg. Chim. Acta* **2009**, *362*, 2467–2474.
[8] a) M. Taki, H. Kumei, S. Itoh, S. Fukuzumi, *J. Inorg. Biochem.* **2000**, *78*, 1–5; b) M. Taki, H. Kumei, S. Nagatomo, T. Kitagawa, S. Itoh, S. Fukuzumi, *Inorg. Chim. Acta* **2000**, *300–302*, 622–632; c) S. Itoh, M. Taki, H. Kumei, S. Takayama, S. Nagatomo, T. Kitagawa, N. Sakurada, R. Arakawa, S. Fukuzumi, *Inorg. Chem.* **2000**, *39*, 3708–3711; d) M. Taki, H. Hattori, T. Osako, S. Nagatomo, M. Shiro, T. Kitagawa, S. Itoh, *Inorg. Chim. Acta* **2004**, *357*, 3369–3381.
[9] a) L. Benisvy, A. J. Blake, D. Collison, E. S. Davies, C. D. Garner, E. J. L. McInnes, J. McMaster, G. Whittaker, C. Wilson, *Chem. Commun.* **2001**, 1824–1825; b) L. Benisvy, A. J. Blake, D. Collison, E. S. Davies, C. D. Garner, E. J. L. McInnes, J. McMaster, G. Whittaker, C. Wilson, *Dalton Trans.* **2003**, 1975–1985; c) L. Benisvy, E. Bill, A. J. Blake, D. Collison, E. S. Davies, C. D. Garner, C. I. Guindy, E. J. L. McInnes, G. McArdle, J. McMaster, C. Wilson, J. Wolowska, *Dalton Trans.* **2004**, 3647–3653; d) L. Benisvy, E. Bill, A. J. Blake, D. Collison, E. S. Davies, C. D. Garner, G. McArdle, E. J. L. McInnes, J. McMaster, S. H. K. Ross, C. Wilson, *Dalton Trans.* **2006**, 258–267.
[10] a) A. dos Anjos, A. J. Bortoluzzi, R. E. H. M. B. Osório, R. A. Peralta, G. R. Friedermann, A. S. Mangrich, A. Neves, *Inorg. Chem. Commun.* **2005**, *8*, 249–253; b) A. dos Anjos, A. J. Bortoluzzi, B. Szpoganicz, M. S. B. Caro, G. R. Friedermann, A. S. Mangrich, A. Neves, *Inorg. Chim. Acta* **2005**, *358*, 3106–3114; c) A. John, M. M. Shaikh, P. Ghosh, *Dalton Trans.* **2008**, 2815–2824.
[11] A. Mukherjee, F. Lloret, R. Mukherjee, *Inorg. Chem.* **2008**, *47*, 4471–4480.
[12] A. W. Addison, T. N. Rao, J. Reedjik, J. van Rijn, G. C. Vershcoor, *J. Chem. Soc., Dalton Trans.* **1984**, 1349–1356.
[13] L. Rodríguez, E. Labisbal, A. Sousa-Pedrares, J. A. García-Vázquez, J. Romero, M. L. Durán, J. A. Real, A. Sousa, *Inorg. Chem.* **2006**, *45*, 7903–7914.
[14] a) J. Reglinski, S. Morris, D. E. Stevenson, *Polyhedron* **2002**, *21*, 2175–2182; b) J. S. Matalobos, A. M. García-Deibe, M. Fondo, D. Navarro, M. R. Bermejo, *Inorg. Chem. Commun.* **2004**, *7*, 311–314.
[15] M. Du, D. L. An, Y. M. Guo, X. H. Bu, *J. Mol. Struct.* **2002**, *641*, 193–198.
[16] I. Castro, J. Sletten, M. L. Calatayud, M. Julve, J. Cano, F. Lloret, A. Caneschi, *Inorg. Chem.* **1995**, *34*, 4903–4909.
[17] O. Kahn, *Molecular Magnetism*, VCH, New York, **1993**.
[18] H. Mishra, R. Mukherjee, *J. Organomet. Chem.* **2007**, *692*, 3248–3260.
[19] V. W. Manner, T. F. Markle, J. H. Freudenthal, J. P. Roth, J. M. Mayer, *Chem. Commun.* **2008**, 256–258.
[20] a) M. Ray, S. Mukerjee, R. Mukherjee, *J. Chem. Soc., Dalton Trans.* **1990**, 3635–3638; b) N. Gupta, S. Mukerjee, S. Mahapatra, M. Ray, R. Mukherjee, *Inorg. Chem.* **1992**, *31*, 139–141; c) M. Ray, D. Ghosh, Z. Shirin, R. Mukherjee, *Inorg. Chem.* **1997**, *36*, 3568–3572; d) A. K. Patra, R. Mukherjee, *Inorg. Chem.* **1999**, *38*, 1388–1393.
[21] S. S. Tandon, S. Chander, L. K. Thompson, J. N. Bridson, V. McKee, *Inorg. Chim. Acta* **1994**, *219*, 55–65.
[22] R. Shukla, P. K. Bharadwaj, J. V. Hall, K. H. Whitmire, *Polyhedron* **1994**, *13*, 2387–2394.
[23] C. K. Williams, L. E. Breyfogle, S. K. Choi, W. Nam, V. G. Young Jr., M. A. Hillmyer, W. B. Tolman, *J. Am. Chem. Soc.* **2003**, *125*, 11350–11359.
[24] D. F. Evans, *J. Chem. Soc.* **1959**, 2003.
[25] a) A. K. Patra, R. Mukherjee, *Inorg. Chem.* **1999**, *38*, 1388–1393; b) A. K. Patra, M. Ray, R. Mukherjee, *Inorg. Chem.* **2000**, *39*, 652–657; c) A. K. Singh, V. Balamurugan, R. Mukherjee, *Inorg. Chem.* **2003**, *42*, 6497–6502 and references cited therein.
[26] L. J. Farrugia, *WinGX version 1.64, An Integrated System of Windows Programs for the Solution, Refinement and Analysis of Single-Crystal X-ray Diffraction Data*, Department of Chemistry, University of Glasgow, **2003**.
[27] R. G. Parr, W. Yang, *Density-Functional Theory of Atoms and Molecules*, Oxford University Press, Oxford, U. K., **1989**.
[28] a) A. D. Becke, *J. Chem. Phys.* **1993**, *98*, 5648–5652; b) C. Lee, W. Yang, R. G. Parr, *Phys. Rev. B* **1998**, *37*, 785–789.
[29] M. J. Frisch, G. W. Trucks, H. B. Schlegel, G. E. Scuseria, M. A. Robb, J. R. Cheeseman, J. A. Montgomery Jr., T. Vreven, K. N. Kudin, J. C. Burant, J. M. Millam, S. S. Iyengar, J. Tomasi, V. Barone, B. Mennucci, M. Cossi, G. Scalmani, N. Rega, G. A. Petersson, H. Nakatsuji, M. Hada, M. Ehara, K. Toyota, R. Fukuda, J. Hasegawa, M. Ishida, T. Nakajima, Y. Honda, O. Kitao, H. Nakai, M. Klene, X. Li, J. E. Knox, H. P. Hratchian, J. B. Cross, C. Adamo, J. Jaramillo, R. Gomperts, R. E. Stratmann, O. Yazyev, A. J. Austin, R. Cammi, C. Pomelli, J. W. Ochterski, P. Y. Ayala, K. Morokuma, G. A. Voth, P. Salvador, J. J. Dannenberg, V. G. Zakrzewski, S. Dapprich, A. D. Daniels, M. C. Strain, O. Farkas, D. K. Malick, A. D. Rabuck, K. Raghavachari, J. B. Foresman, J. V. Ortiz, Q. Cui, A. G. Baboul, S. Clifford, J. Cioslowski, B. B. Stefanov, G. Liu, A. Liashenko, P. Piskorz, I. Komaromi, R. L. Martin, D. J. Fox, T. Keith, M. A. Al-Laham, C. Y. Peng, A. Nanayakkara, M. Challacombe, P. M. W. Gill, B. Johnson, W. Chen, M. W. Wong, C. Gonzalez, J. A. Pople, *Gaussian 03*, Gaussian Inc., Wallingford, CT, **2004**.
[30] Gaussian Inc., Wallingford, CT, **2004**.

Received: August 3, 2009
Published Online: January 27, 2010

